

## Multistage Enrichment of the Sawafuqi Uranium Deposit: New Insights into Sandstone-hosted Uranium Deposits in the Intramontane Basins of Tian Shan, China

LIU Zhangyue<sup>1,2</sup>, PENG Suping<sup>1,\*</sup>, QIN Mingkuan<sup>2</sup>, LIU Hongxun<sup>2</sup>, HUANG Shaohua<sup>2</sup>, HE Zhongbo<sup>2</sup>, GUO Qiang<sup>2</sup>, XU Qiang<sup>2</sup> and SONG Jiye<sup>2</sup>

<sup>1</sup> State Key Laboratory of Coal Resources and Safe Mining, China University of Mining and Technology, Beijing 100083, China

<sup>2</sup> Beijing Research Institute of Uranium Geology, China National Nuclear Corporation (CNNC), Beijing 100029, China

**Abstract:** Meso-Cenozoic intracontinental orogenic processes in the Tian Shan orogenic belt have significant effect on the sandstone-hosted uranium deposits in the intramontane basins and those adjacent to the orogen. The Sawafuqi uranium deposit, which is located in the South Tian Shan orogenic belt, is investigated to reveal the relationships between uranium mineralization and orogenies. Recent exploration results show that the Sawafuqi uranium deposit has tabular, stratiform, quasi-stratiform, and lens-like orebodies and various geological characteristics different from typical interlayer oxidation zone sandstone-hosted uranium deposits. Systematic studies of ore samples from the Sawafuqi uranium deposit using a variety of techniques, including thin section observation,  $\alpha$ -track radiograph, electron microprobe and scanning electron microscope, suggest that uranium mineralization is closely related to pyrite and organic matter. Mineralization-related alterations in the host rocks are mainly silicification and argillation including kaolinite, illite (and illite-smectite mixed layer) and chlorite. Three stages of mineralization were identified in the Sawafuqi uranium deposit: (i) uranium-bearing detritus and symsedimentary initial pre-enrichment; (ii) interlayer oxidization zone uranium mineralization; and (iii) vein-type uranium mineralization. The symsedimentary uranium pre-enrichment represents an early uranium enrichment in the Sawafuqi uranium deposit, and interlayer oxidation zone uranium mineralization formed the main orebodies, which are superimposed by the vein-type uranium mineralization. Combining the results of this study with previous studies on the Meso-Cenozoic orogenies of South Tian Shan, it is proposed that the symsedimentary uranium pre-enrichment of the Sawafuqi uranium deposit was caused by Triassic Tian Shan uplift, and the interlayer oxidation zone uranium mineralization occurred during the Eocene-Oligocene period, when tectonism was relatively quiet, whereas the vein-type uranium mineralization took place in relation to the strong orogeny of South Tian Shan since Miocene.

**Key words:** South Tian Shan, intracontinental orogeny, Sawafuqi uranium deposit, multistage uranium mineralization

### 1 Introduction

Typical sandstone-hosted uranium orebodies formed by interlayer oxidation are roll- or quasi-roll-shaped and were first described in the Colorado Plateau, U.S.A (Wright, 1955; Shawe, 1956), with the uranium grade in the ores ranging from 0.02% to 0.07% (OECD, 2008). Generally,

during diagenesis, hexavalent uranium is reduced by organic matter and pyrite formed in the sandstones, organic acids produced in mudstones, and oil and gas ascended from the deeper parts of basins, and uranium minerals precipitate, forming tabular or roll-shaped uranium orebodies along the redox front (Granger et al., 1961; Saucier, 1980; Turner-Peterson and Fishman, 1986). Organic matter present in the form of hydrocarbons can produce secondary reduction and enrichment of high-

\* Corresponding author. E-mail: psp@cumtb.edu.cn

grade uranium ores (Crawley et al., 1985; Granger and Santos, 1986; Rieger et al., 2008; Beata et al., 2009; Fuchs et al., 2015). For example, sandstone-hosted uranium deposits in the northeastern Ordos Basin, China, underwent multistage uranium mineralization, including phreatic oxidation, interlayer oxidation, and modification by hydrocarbon-bearing fluids that enriched the uranium ores (Li et al., 2005; 2006). The mixing of fluids from different sources and, especially, the uranium mineralization owing to hydrothermal fluids, has attracted attention of a number of researchers (Li Ziyang et al., 2006; Wu et al., 2007; Du Letian and Ou Guangxi, 2007; Nie Fengjun et al., 2010; Chi and Xue, 2014; Jin Ruoshi et al., 2014; Zhang Chengyong et al., 2015; Cao et al., 2016; Jiao et al., 2016; Bonnetti et al., 2017; Zhang et al., 2017).

The South Tian Shan orogeny started with the collision between the Tarim and Junggar blocks in Late Devonian–Early Permian, with multistage uplift and erosion since then (Gao et al., 1998; Bullen et al., 2001; He Guoqi et al., 2001; Shu et al., 2002; Biske and Seltnann, 2010; Han et al., 2010; Charvet et al., 2011). The stress state that fluctuated between compression and relaxation formed the structural–metamorphic–hydrothermal metallogenetic system. Large-scale mineralization occurred during the orogeny (Zhai Yusheng, 1996; Deng Jun et al., 2000; Hou Zengqian, 2010). Fluids originating from the junction between the orogen and the foreland basin carried heat, metallic elements and organic matter migrated to the basin and formed huge metal sulfide deposits as well as stratabound sandstone-hosted uranium deposits at the basin edge (Mitchell and Garson, 1981; Oliver, 1992; Hou Zengqian et al., 2004; Leach et al., 2005). Thus, the Tian Shan Mountain uplift in the Mesozoic and Cenozoic have been related to the formation of intramontane basins as well as the generation of mineral deposits such as sandstone-hosted uranium and stratabound Pb–Zn deposits (Hendrix, 2000; Bullen et al., 2001; Smieja-Król, et al., 2009). Although the uranium mineralization in the Chu-Sarysu and Syr Darya basins in south-central Kazakhstan has been attributed to the Tian Shan orogeny (Jaireth et al., 2008; Chi and Xue, 2014), few have studied the role of orogeny-related hydrothermal activity in the sandstone-hosted uranium deposits.

The Sawafuqi uranium deposit in South Tian Shan is the only large-scale sandstone-hosted uranium deposit in the Jurassic strata in China. Recent exploration results have shown that the deposit comprises tabular, stratiform, quasi-stratiform, and lens-like orebodies that differ from typical sandstone-hosted uranium deposits (Fang Minqiang, 2010; Wu Kongyun et al., 2010). The ore thicknesses and grades gradually increase downward, with uranium grade higher than 1.0% in some sandy conglomerate-type ores (Liu

Zhangyue, 2008a; Shen Pingxi, 2010a). However, no consensus has been reached on the genesis of the deposit. Most researchers believe that the orebodies formed at the interlayer oxidation front and their spatial distribution is controlled via lithology and the oxidation zone (Wu Kongyun et al., 2010; Shen Pingxi, 2010b; Lin Xiaobin et al., 2013). Others, however, argue that the uranium mineralization is mainly controlled by pyrite and organic matter, and the uranium deposit may be associated with oil and gas (Chen Hongbin et al., 2007). In this paper, detailed petrographic analysis of the ores and host rocks was carried out in combination with  $\alpha$ -track radiography, electron microprobe analysis (EPMA), and scanning electron microscopy (SEM), in order to study the mechanisms of enrichment of the Sawafuqi uranium deposit. The paper aims to study the role of orogeny in the formation of the Sawafuqi uranium deposit and, specifically, the relation between intracontinental orogeny and sandstone-hosted uranium deposits.

## 2 Metallogenic Background

The Sawafuqi uranium deposit is located in the Kurgan Intramontane Basin, in the South Tian Shan orogenic belt. The Kurgan Intramontane Basin is the result of the continuous evolution of the Tarim Basin owing to the collision of the Yining–Central Tian Shan landmass and the Tarim Plate in Late Paleozoic (Zhu et al., 2008; Gao et al., 2011). This 58 km long (EW) and 2–4 km wide (NS) basin was initially a part of the Tarim Basin and became an intramontane basin separated from the Tarim Basin during the uplift of the region. The Kurgan Basin is bound by a piedmont fault (F1) to the north, where Carboniferous (C) strata and Hercynian granites ( $\gamma_4^3$ ) are exposed, and by the Mansuertage Uplift and the Sinian Sawafuqi Group ( $Z_{1sw}$ ) to the south bordering the Tarim Basin. The Lower Permian Xiaotikanlike Formation ( $P_{1x}$ ), in the southwest of the Kurgan Basin, is dominated by volcanic rocks. The basement comprises Carboniferous and Lower Permian rocks. The basin cover includes the Middle–Upper Triassic Xiaoquanguo Formation ( $T_{2-3xq}$ ), the Jurassic (J) and Lower Cretaceous Yageliemu Formation ( $K_{1y}$ ), the Pliocene Atushi Formation ( $N_{2a}$ ), and Quaternary diluvial and glacial sediments ( $Q_{3-4}$ ) (Liu Zhangyue et al., 2011) (Fig. 1).

The northern boundary of the Kurgan Intramontane Basin is marked by the F1 fault, which runs through the northern margin of the Tarim Basin and constitutes the boundary between the Tarim Plate and South Tian Shan. The fault not only controls the piedmont slope but also affects the monoclinical structures of the northern Tarim Basin. The piedmont slope, through controlling the

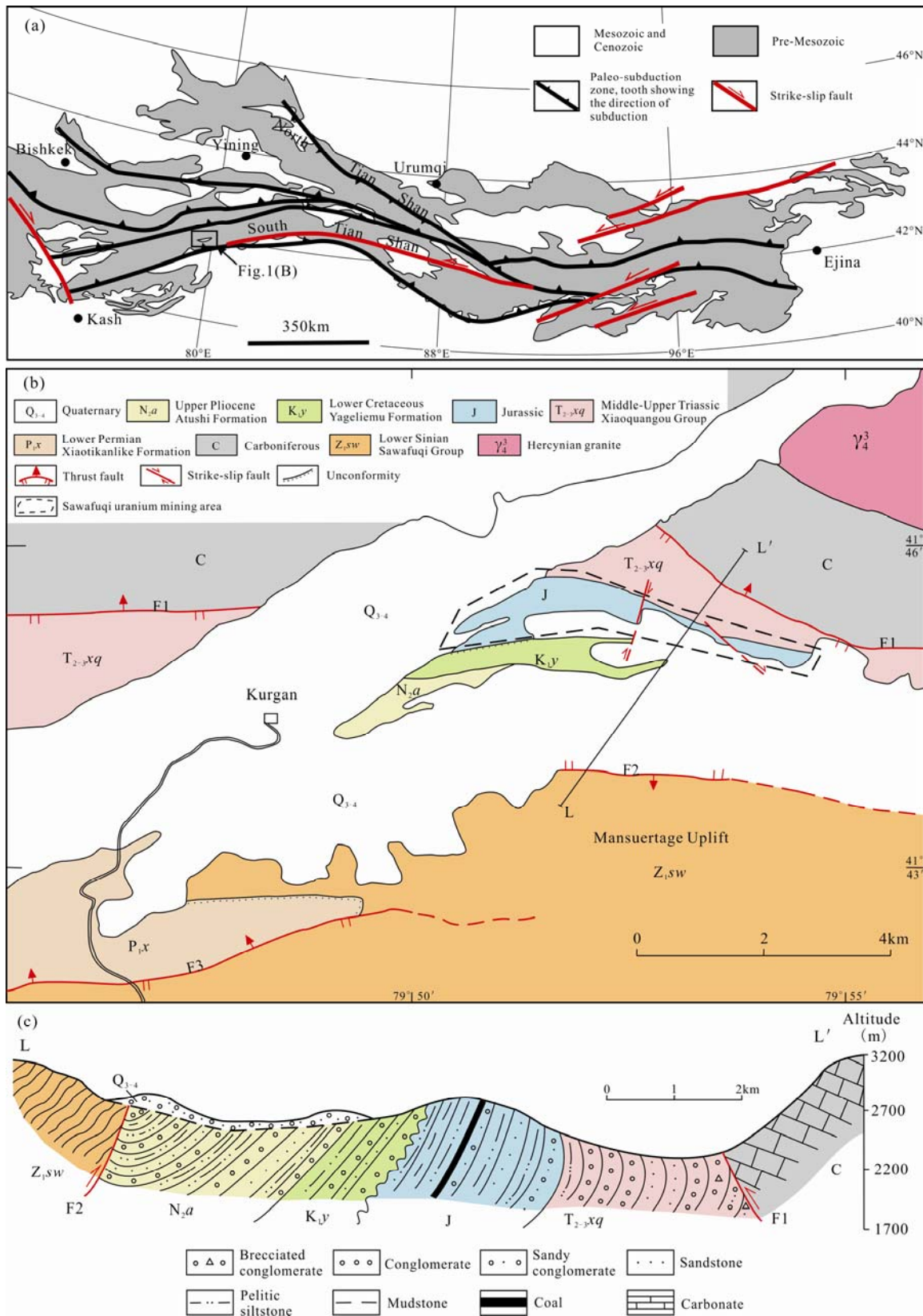


Fig. 1. (a). General tectonic map of the Tianshan orogenic belt and adjacent areas (modified from Gao et al., 2011; Yang et al., 2017); (b). Geological map of the Kurgan Intramontane Basin and location of the Sawafuqi uranium deposit; (c). Cross section of the Sawafuqi uranium deposit (modified from Liu Zhangyue et al., 2008a).

groundwater flowing from South Tian Shan, is critical to the formation of the sandstone-hosted uranium deposits. The southern boundary of the Kurgan Intramontane Basin is controlled by the F2 thrust fault that has an intermittently exposed fault plane along strike. The F1 and F2 faults control the formation and evolution of the Kurgan Intramontane Basin and are critical to the formation of the Sawafuqi uranium deposit.

The Jurassic sequence, which has a maximum thickness of more than 700 m, is composed of the Lower Jurassic Qixingbulake Formation, the Middle-Upper Jurassic Tiemiersu Formation and the Upper Jurassic Qigu Formation (Fig. 2). The 240-m-thick Qixingbulake Formation is composed of conglomerates, sandy conglomerates, and interbedded medium- to coarse-grained sandstones. A sequence of thick-bedded conglomerates marks the base of this formation, with poor roundness and sorting, representing alluvial fan sediment. The Tiemiersu Formation has a thickness of 245 m and is divided into two members ( $J_{2-3}tm^1$  and  $J_{2-3}tm^2$ ). The 89-m-thick lower member is mainly interbedded by conglomerates, sandy conglomerates, medium-grained sandstones and mudstones in unequal thickness, with two thin coal seams. Cross-beddings are observed locally. The 156-m-thick upper member is characterized by three thick-bedded sandy conglomerate sequences of braided river and three sandy mudstone sequences of swamp with interbedded carbonaceous shales and two thick coal seams. The Tiemiersu Formation can be divided into five coarse-to-fine sedimentary cycles. The Qigu Formation is composed of 216-m-thick red mudstones of lacustrine facies, with a base of thin-bedded sandy conglomerates and sandstones. Horizontal beddings were observed.

### 3 Uranium Mineralization

The Sawafuqi uranium deposit is hosted in the coal-bearing clastic rocks of the Middle–Lower Jurassic Tiemiersu Formation, where ten uranium orebodies from south to north are located and four industrial grade uranium orebodies are developed (UII-1, UII-2, UII-3 and UII-4) (Fig. 2). The ore-bearing rocks are predominantly conglomerates and coarse, medium, and fine sandstones. The host sandstones contain abundant carbonaceous debris (Fig. 3a), organic matter veins (Fig. 3b) and pyrite (Fig. 3c). Total organic carbon is 0.50%–0.54% and total sulfur is 0.35%–0.39% (Liu Zhangyue et al., 2008b).

Cracks are common in the host rocks owing to the F1 Fault and are filled by both silica-rich and organic material, especially between the sandstones and coal beds. The silica-rich veins in the coal seams are strongly deformed. The veins filled with organic material in the

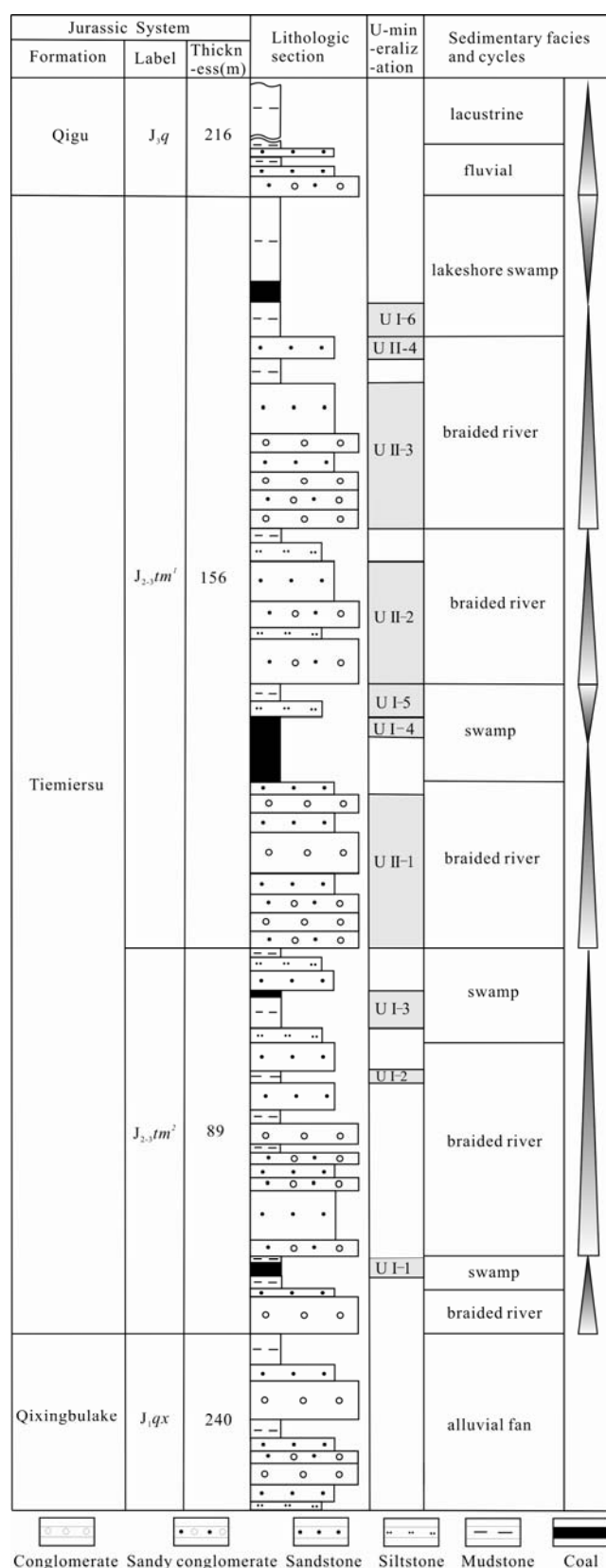


Fig. 2. Generalized stratigraphic column of the Jurassic strata in the Sawafuqi uranium deposit (modified from Liu Zhangyue et al., 2008a).

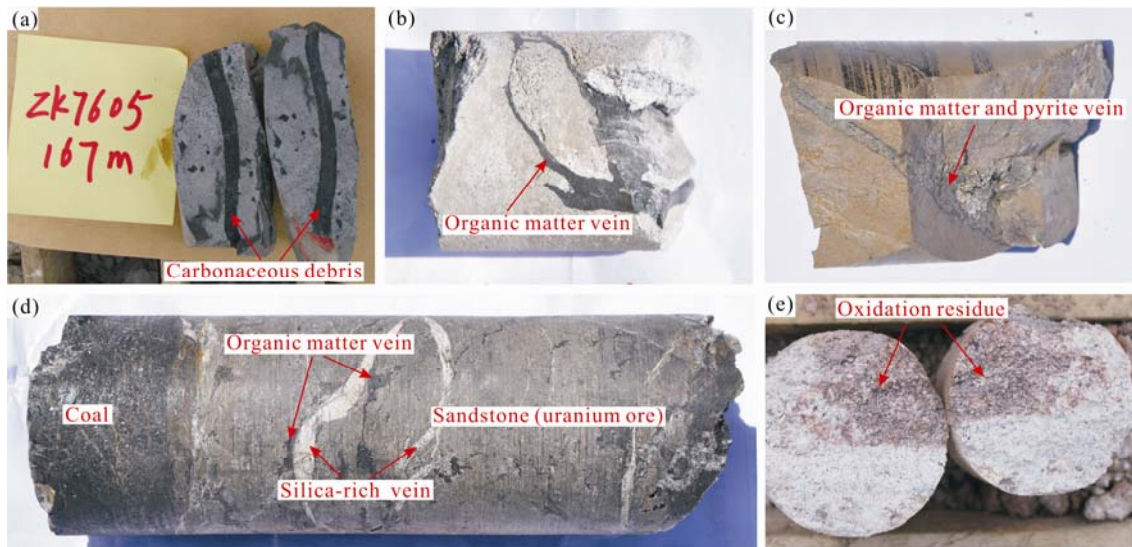


Fig. 3. Characteristics of host rocks in the Sawafuqi uranium deposit.

(a), Carbonized plant debris in the sandstone. (b), Organic matter vein filling the crack in the greyish-white sandstone. (c), Organic and pyrite vein filling a crack in siltstone. (d), Silica-rich veins cutting through organic matter veins in the ore-bearing sandstone. (e), Oxidation residues in the bleached sandstone.

sandstones are cut by silica-rich veins (Fig. 3d). The uranium mineralization is closely related to the organic material and pyrite. The ore beds are steeply inclined  $55^{\circ}$ – $85^{\circ}$  and are reversed in the northern mining area.

Compared with typical sandstone-hosted uranium deposits with obvious red interlayer oxidation zones, no clear red or yellow oxidation zones are present in the host sandstones. However, there are numerous yellowish red residual oxidation stripes or spots in the grayish white host rocks (Fig. 3e). The orebodies are stratiform, quasi-stratiform, tabular, with variable thicknesses, and few are lenticular, but no roll-shaped orebodies are present (Fig. 4). EW-striking uranium mineralization is present in EW-striking sandstones adjacent to mudstones or coal seams.

Uranium mainly exists as absorbed uranium and uranium minerals. Uranium is mainly absorbed by organic matter, iron-titanium oxides, and clay minerals. Uraninite is common and is associated with poorly crystalline pyrite and organic-matter-filled veins (Chen Hongbin et al., 2007; Shen Pingxi, 2010a).

## 4 Sample Collection and Analytical Methods

### 4.1 Sample collection

Ore-bearing sandstone and conglomerate samples from drill (cutting through UII-1 and UII-2) cores were collected. An HD-2000 hand-held gamma radiometer, manufactured by the Beijing Research Institute of Uranium Geology, CNNC, was used to first scan samples from drill cores. The scanning time was 10 s, and ore-bearing samples with more than  $30 \text{ nC}\cdot\text{kg}^{-1}\cdot\text{h}^{-1}$  (Gamma radiation exposure rate) were collected.

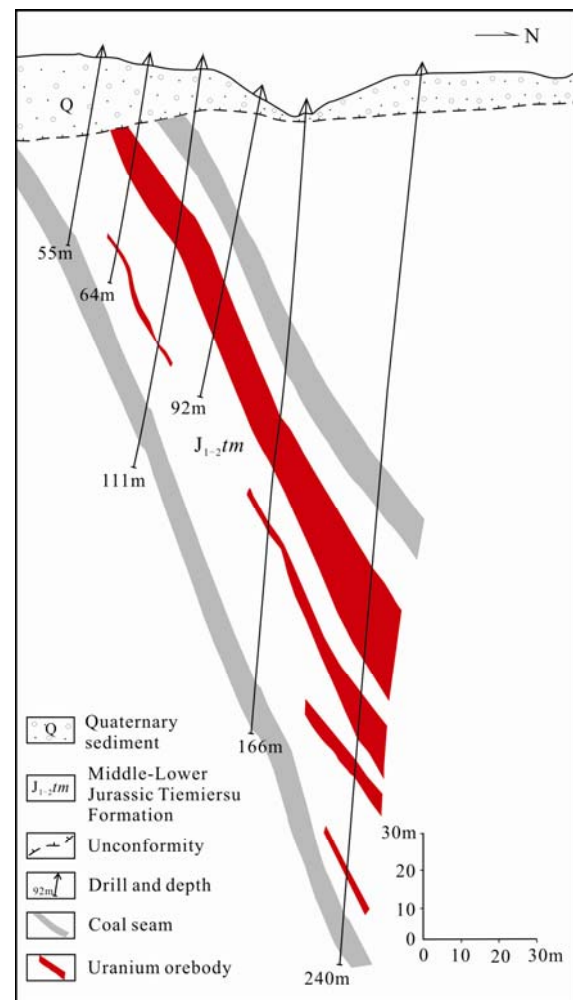


Fig. 4. A cross section of the Sawafuqi uranium deposit.

## 4.2 Analytical methods

First, the caked mud on the surface of the drill core samples was removed. Then, the samples were washed with distilled water, and then cut and polished into thin sections roughly 0.05 mm thick. A Carl Zeiss Axioskop 40 polarizing microscope was used to study the polished thin sections. Thin sections rich in uranium minerals were further examined with EPMA using a JXA-8100 microprobe (JEOL Ltd.). ZAF corrections were used for the correction procedure. The operating conditions were: acceleration voltage 20 kV, current intensity 10 nA, and beam diameter 1  $\mu\text{m}$ .

After EPMA, the carbon-coated thin sections were polished again to remove the carbon coating, cleaned with alcohol, and dried in air. Nuclear emulsions were evenly applied to the clean and dry thin sections in a darkroom before placing into a black case for  $\alpha$ -track formation (approximately 15 days). Finally, the  $\alpha$ -track distribution, density, and pattern were observed under a microscope.

Sample processing and analysis were conducted at the Beijing Research Institute of Uranium Geology, CNNC. Uranium minerals in sandstone-hosted uranium deposits are relatively microcrystalline and commonly fill the intergranular pores. They are easily damaged and difficult to preserve during grinding. Thus, in this study, in situ SEM was used to study the uranium ores at the Research Institute of Petroleum Exploration & Development's Experimental Research Center. First, areas with relatively well-developed veins filled with organic matter, pyrite, and clay minerals that are closely related to uranium minerals were selected for SEM EDS analysis using a TESCAN-VEGA II LMU SEM with a LINK-ISISX alpha particle spectrometer. The SEM was operated at 15 kV in high-vacuum mode, with manual aperture and 4.5 beam spot size. To improve the quality of the analyses, all the samples were covered by sputtering a thin Au coat to ensure surface conductivity.

## 5 Results

### 5.1 Uranium ore mineralogy

The detrital grains of the sandstone ores are mainly composed of metamorphic and igneous quartz, generally brown and occasionally mottled by iron staining, as single crystals or polycrystalline aggregates with compaction fractures (Fig. 5a). There is also authigenic quartz that occasionally overgrows detrital quartz grains (Figs. 5b and 5c), presumably owing to silica-rich or acidic fluids. Feldspar grains were rarely observed. Metamorphic rock and volcanic tuffaceous detritus (e.g., sandy mudstone, argillaceous sandstone, slates, granites, volcanic tuff) are present.

Pyrite is commonly found in the cement or carbonaceous debris and is roughly divided into two types based on crystal morphology. Crystalline pyrite forms cubes, pentagonal dodecahedra (Fig. 5d), and strawberry-like grains (Fig. 5e) and mainly coexists with organic matter, finely dispersed in the cement and intergranular pores. The cubic pyrite occasionally has uraninite in the center (Fig. 5f). Subhedral pyrite is observed in intergranular pores and cement particles (Fig. 5g), and is closely associated with uranium mineralization.

Carbonized plant debris, with visible plant cellular structure (Fig. 5h), is parallel to bedding. In contrast, externally derived organic matter is present in veins and cracks (Fig. 5i), filling the intergranular pores and microcracks that cut the bedding. Carbonaceous debris is common in the sandstones, whereas organic matter veins are relatively common in the mineralized conglomerates and sandstones.

Uraninite is the dominant uranium mineral, and uranium is also absorbed in clays and carbonaceous debris. Based on  $\alpha$ -track radiography, the  $\alpha$ -tracks generated by the absorbed uranium are relatively short, sparse, and disorderly (Figs. 5j and 5k). In contrast, the  $\alpha$ -tracks generated by uraninite form a dense radial pattern around the uranium minerals (Fig. 5l).

### 5.2 Alteration and uranium mineralization

#### 5.2.1 Clay alteration

Feldspar and mica minerals in the ore-bearing sandstone are replaced by clay minerals. The alteration types are kaolinization, illitization (mixed illite-smectite), and chloritization.

Kaolinization is common in all ores. It is associated with the cement and occasionally with pyrite and iron-stained spots. Kaolinite in intergranular pores is flaky and vermicular (Fig. 6a). Most kaolinite grains cover the surface of quartz or are distributed in feldspar dissolution pores (Fig. 6b). Kaolinization generally indicates the acidified front of the interlayer oxidation zone, spatially close to the redox front (Devoto, 1978; Harshman, 1972).

Illite and smectite commonly occur in mixed layer with disseminated pyrite that is locally oxidized and iron-stained. Illitization affects the carbonaceous debris and quartz, and is associated with uranium minerals (Fig. 6c). SEM analysis suggests that illite replaces K-feldspar and is observed on detrital grain surfaces and filling intergranular pores (Fig. 6d). Illitization is associated with the oxidation zone or the redox front. The ore-forming acidic fluids may have changed to alkaline as the oxidizing uranium-bearing fluids migrate to the reduced zone. Illitization is referred to be produced in this transition that signifies the commencement of uranium

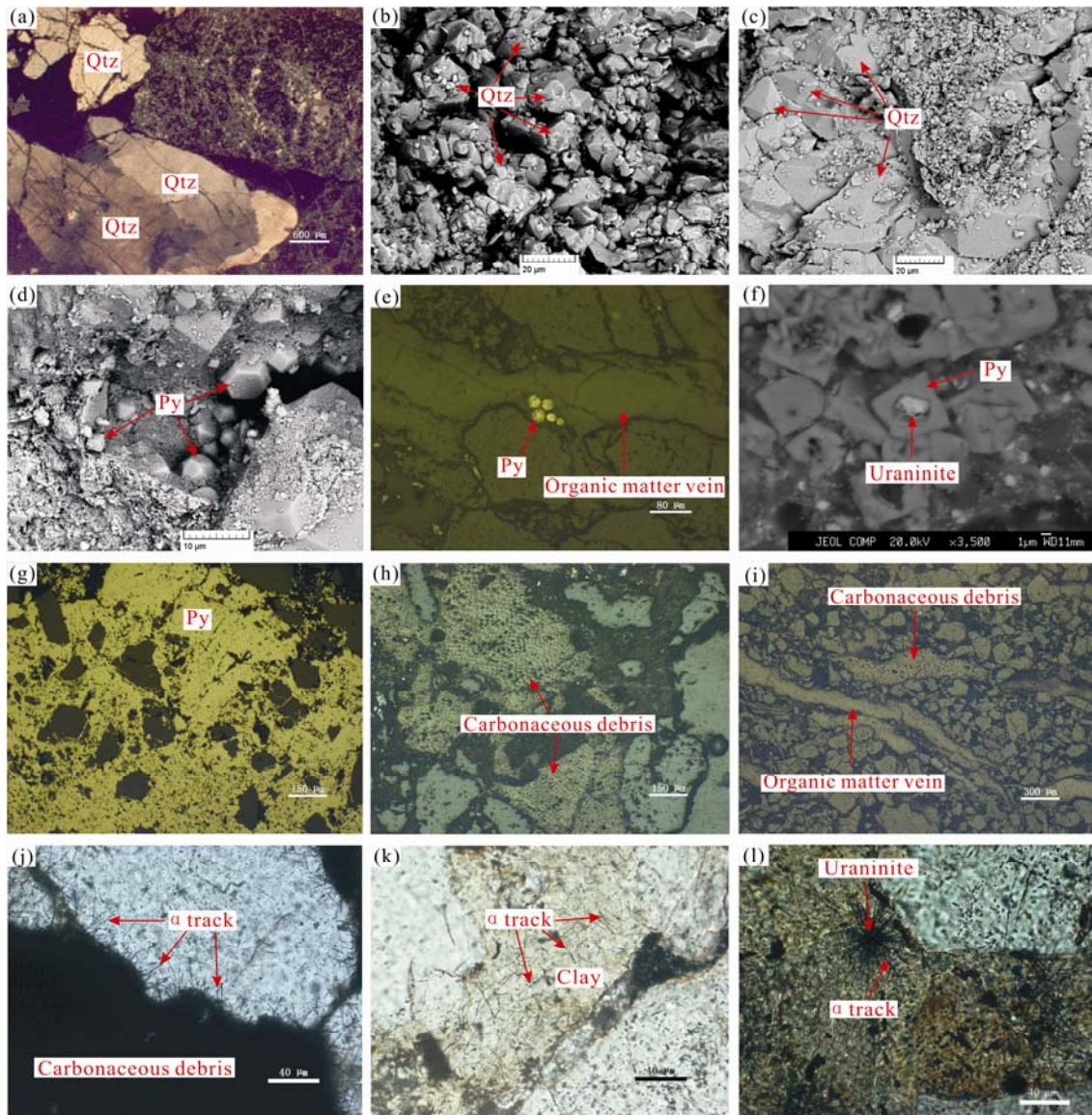


Fig. 5. Typical minerals and their occurrences in the uranium ore.

(a), Metamorphic quartz with compaction fractures. (b), Intergranular authigenic quartz. (c), Quartz overgrowth to level III. (d), Intergranular cubic and dodecahedral pyrite. (e), Strawberry-like pyrite coexisting with organic matter vein. (f), Uraninite in the center of pyrite. (g), Subhedral pyrite cementing detrital grains. (h), Carbonized plant debris in the sandstone. (i), Organic matter vein filling fractures in sandstone. (j),  $\alpha$ -tracks generated by the absorbed uranium in the carbonaceous debris. (k),  $\alpha$ -tracks generated by the absorbed uranium in the clay minerals. (l),  $\alpha$ -track pattern of uraninite. Qtz, Quartz; Py, Pyrite.

mineralization (Aleksandre et al., 2005; Polito et al., 2006).

Chlorite is fibrous and replaces intergranular matrix (Fig. 6e), carbonate cements (Fig. 6f) and mixed illite-smectite (Fig. 6g). Based on the sequence of metasomatic minerals, chloritization occurs after kaolinization and illitization, and is commonly the product of epithermal alteration (Nutt, 1989; Komninou and Sverjensky, 1995; Li et al., 2007; Zhang et al., 2017).

### 5.2.2 Silica-rich veins

Silica-rich veins, consisting of microcrystalline or amorphous quartz, are common in the host rocks and are

observed in the intergranular pores, cement, and fractured detritus. The silica-rich veins are impure and may contain pyrite, clay minerals, and uraninite (Fig. 6h). SEM images show that such silica-rich veins consist of amorphous quartz and uraninite (Figs. 6i and 6j). The silica-rich veins cut the organic matter veins (Fig. 6k), the clay minerals or string-shaped uraninite veins (Fig. 6l), and clearly formed after the main uranium mineralization.

### 5.3 Uranium mineralization

Three stages of uranium mineralization were identified in the Sawafuqi uranium deposit: (i) uranium-bearing

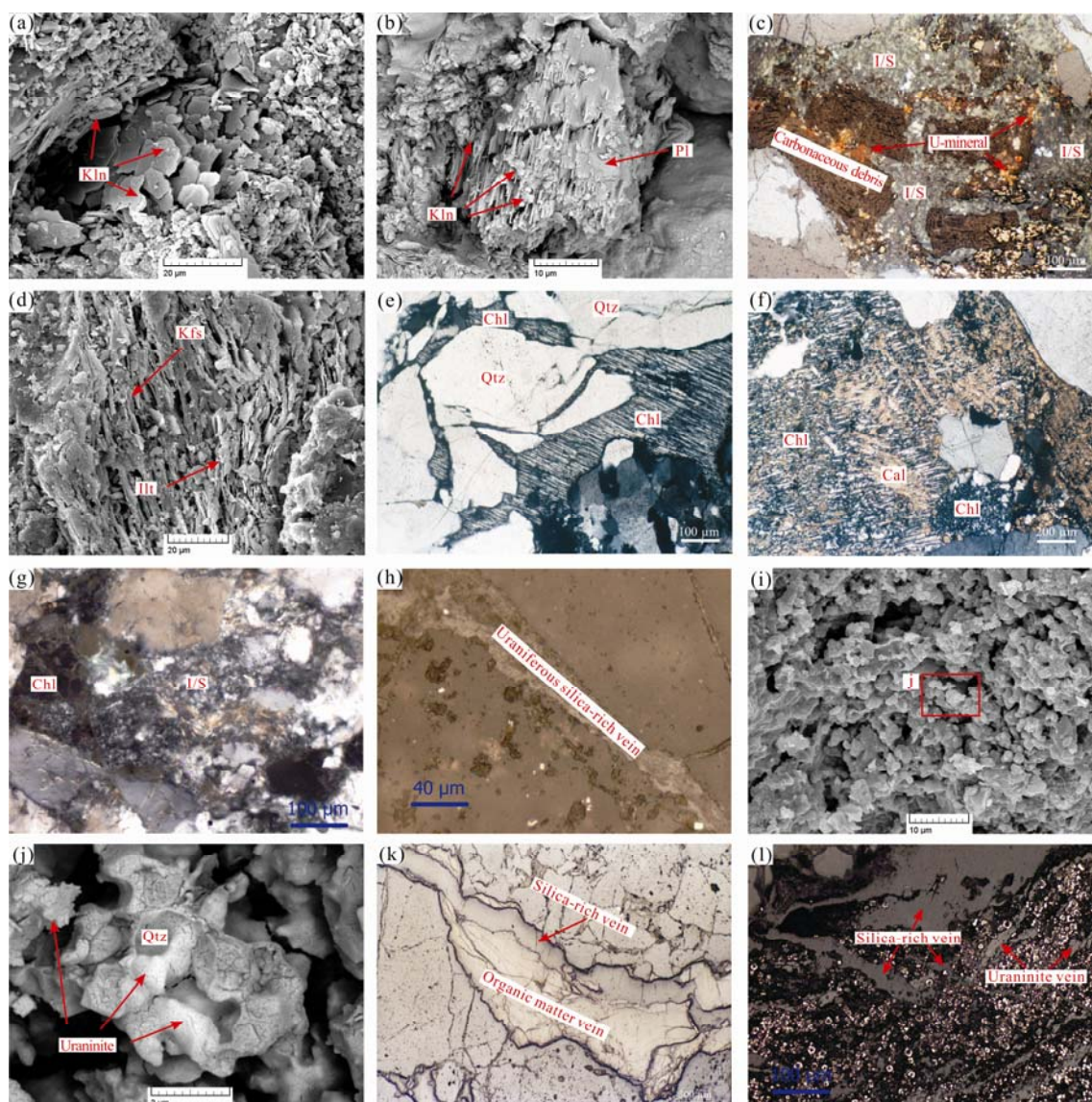


Fig. 6. Alteration minerals and their morphology in the uranium ore.

(a), Irregular kaolinite filling intergranular pores. (b), Kaolinite replacing plagioclase. (c), illite/smectite mixed layer replacing carbonaceous debris in association with the precipitation of uranium minerals. (d), Illite replacing K-feldspar. (e), Fibrous chlorite replacing intergranular matrix. (f), Fibrous chlorite replacing carbonate cements; (g), Chlorite replacing illite/smectite mixed layer. (h), Uraniferous silica-rich vein filling the intergranular pores and fractures. (i), SEM image of uraniferous silica-rich vein. (j), Uraninite precipitating around quartz. (k), Organic matter vein cut by silica-rich vein. (l), Uraninite vein cut by silica-rich vein with brightly scattered pyrite. Kln, Kaolinite; Pl, Plagioclase; I/S, Illite/smectite mixed layer; Ill, Illite; Kfs, K-feldspar; Chl, Chlorite; Qtz, Quartz; Cal, Carbonate.

detritus and syndimentary pre-enrichment; (ii) interlayer oxidation zone uranium mineralization; and (iii) vein-type uranium mineralization.

### 5.3.1 Syndimentary uranium pre-enrichment

Syndimentary uranium pre-enrichment is attributed to the sedimentation of uranium-bearing detritus. The uranium-bearing detritus comprises metamorphic quartz and slate grains, and is attributed to denudation, transport, and sedimentation from preexisting uranium deposits in the source area. Within the uranium-bearing detritus, uraninite exists as microparticles or aggregates (Figs. 7a–7c). Compared with epigenetic infiltration-type uranium

mineralization that forms either string-shaped uraninite that fills intergranular pores or fractures or massive uraninite that precipitates around reducing agents, the detrital uraninite is sparse and does not fill fractures. Thus, such uraninite grains do not belong to the infiltration-type uranium mineralization and are likely transported from the provenances. EPMA analysis shows that the  $\text{UO}_2$  content in these uraninite grains is between 78.1% and 92.9%,  $\text{SiO}_2$  is between 0.6% and 10.0%, FeO is between 0.5% and 0.6%, and there are small amounts of K, Na, Y, Ca, Ti, and P. Totals of the analyzed elements are between 98.3% and 100% (Table 1). In general, this type of uraninite is relatively pure.

Table 1 Electron microprobe analysis data of uraninite and pyrite grains in three uranium mineralization stages (wt%)

Mineralization stages	Measurement point	Na <sub>2</sub> O	SiO <sub>2</sub>	K <sub>2</sub> O	UO <sub>2</sub>	As <sub>2</sub> O <sub>5</sub>	MgO	FeO	SO <sub>3</sub>	Al <sub>2</sub> O <sub>3</sub>	PbO	TiO <sub>2</sub>	Y <sub>2</sub> O <sub>3</sub>	CaO	ThO <sub>2</sub>	Cr <sub>2</sub> O <sub>3</sub>	P <sub>2</sub> O <sub>5</sub>	MnO	Total (%)
Syndimentary uranium pre-enrichment	Fig. 7c-1	0.4	10.0	0.3	78.1	0.1	0.3	0.5	0.9	0.2	0.1	1.8	0.2	2.8	-	0.9	1.7	-	98.3
	Fig. 7c-2	0.5	0.6	0.3	92.9	0.2	0.1	0.6	0.3	0.1	-	1.2	0.5	1.5	-	-	1.1	0.1	100.0
	Fig. 7d-1	1.3	3.5	0.6	59.6	0.2	0.2	5.5	4.5	0.2	0.8	1.7	0.1	1.4	1.1	0.3	1.0	0.1	82.1
Interlayer oxidization zone uranium mineralization	Fig. 7e-1	-	-	-	-	0.1	-	41.4	48.9	-	0.1	0.8	-	-	-	-	-	-	91.3
	Fig. 7e-2	0.4	1.9	0.3	53.2	0.2	0.1	11.1	14.2	1.6	0.1	1.0	0.2	0.8	-	0.2	1.1	-	86.4
	Fig. 7e-3	0.5	4.3	0.2	57.9	-	0.5	6.6	2.2	0.2	-	0.1	0.6	0.2	-	1.0	0.2	0.3	74.8
Vein-type uranium mineralization	Fig. 7h-2	0.4	3.2	0.5	87.7	0.1	0.1	0.7	0.5	0.2	-	3.6	0.1	0.6	-	-	0.5	0.1	98.3
	Fig. 7i-3	-	-	-	-	0.6	-	41.0	47.2	-	-	0.8	-	-	-	-	-	-	89.6
	Fig. 7i-4	-	-	-	-	0.8	-	39.5	46.8	-	-	0.9	-	-	-	-	-	-	88.0
	Fig. 7i-5	0.2	5.2	0.4	72.5	0.2	0.1	4.2	0.9	3.3	0.3	2.7	0.1	0.7	-	0.1	1.1	-	92.0
	Fig. 7i-6	0.4	2.1	0.3	84.8	0.1	0.1	3.1	0.8	0.5	0.3	2.9	0.2	0.2	-	0.2	0.7	0.1	97.4

### 5.3.2 Interlayer oxidization zone uranium mineralization

The interlayer oxidization zone mineralization is the most common mineralization type in the Sawafuqi uranium deposit. Uraninite aggregates commonly fill the intergranular pores, forming strings of single particles of several  $\mu\text{m}$  (Fig. 7d). Uranium mineralization is closely related to pyrite and carbonized plant debris. Uraninite precipitates around pyrite (Fig. 7e) and carbonaceous debris (Fig. 7f), and fills the plant cells (Fig. 7g). EPMA analysis shows that the UO<sub>2</sub> content in such type of uraninite is between 53.2% and 59.6%, SiO<sub>2</sub> is between 1.9% and 4.3%, FeO is between 5.5% and 11.1%, and there are small amounts of K, Na, Al, Y, Ca, P, and Cr. Due to the small size of the uranium minerals, the totals of the analyzed elements, affected by surrounding gaps or carbonaceous debris, are between 74.8% and 86.4%, much lower than 100% (Table 1). Compared with syndimentary uraninite, the purity of the uraninite formed in this stage is low, with markedly high Fe and low Si contents.

### 5.3.3 Vein-type uranium mineralization

The vein-type uranium mineralization is closely associated with the silica-rich veins. Fine uraninite grains are dispersed in the silica-rich veins (Fig. 6j). In addition, the irregular uraninite aggregates associated with intrusion of the organic matter veins occasionally fill the intergranular pores and cement the debris (Fig. 7h). Furthermore, the uraninite and pyrite grains are part of the cement, in which uraninite forms block in cubic pyrite or intermingles with poorly crystallized pyrite (Fig. 7i). EPMA analysis shows that the UO<sub>2</sub> content in these uraninite grains is between 72.5% and 87.7%, SiO<sub>2</sub> is between 2.1% and 5.2%, FeO is between 0.7% and 4.2%, TiO<sub>2</sub> is between 2.7% and 3.6%, and there are small amounts of K, Na, Al, Ca, and P. Totals of analyzed elements are between 92.0% and 98.3% (Table 1). Compared with the interlayer oxidization zone uranium mineralization, this type of uraninite has high U purity, low Fe, and high Ti contents.

## 6 Discussion

### 6.1 Uranium mineralization sequence

Based on the above, the formation sequence of uranium and alteration minerals is listed in Table 2. It can be concluded an obvious formation sequence among the alteration minerals and three uranium mineralization stages.

A large number of well-rounded and uranium-bearing detrital grains are present in the host rocks, in which

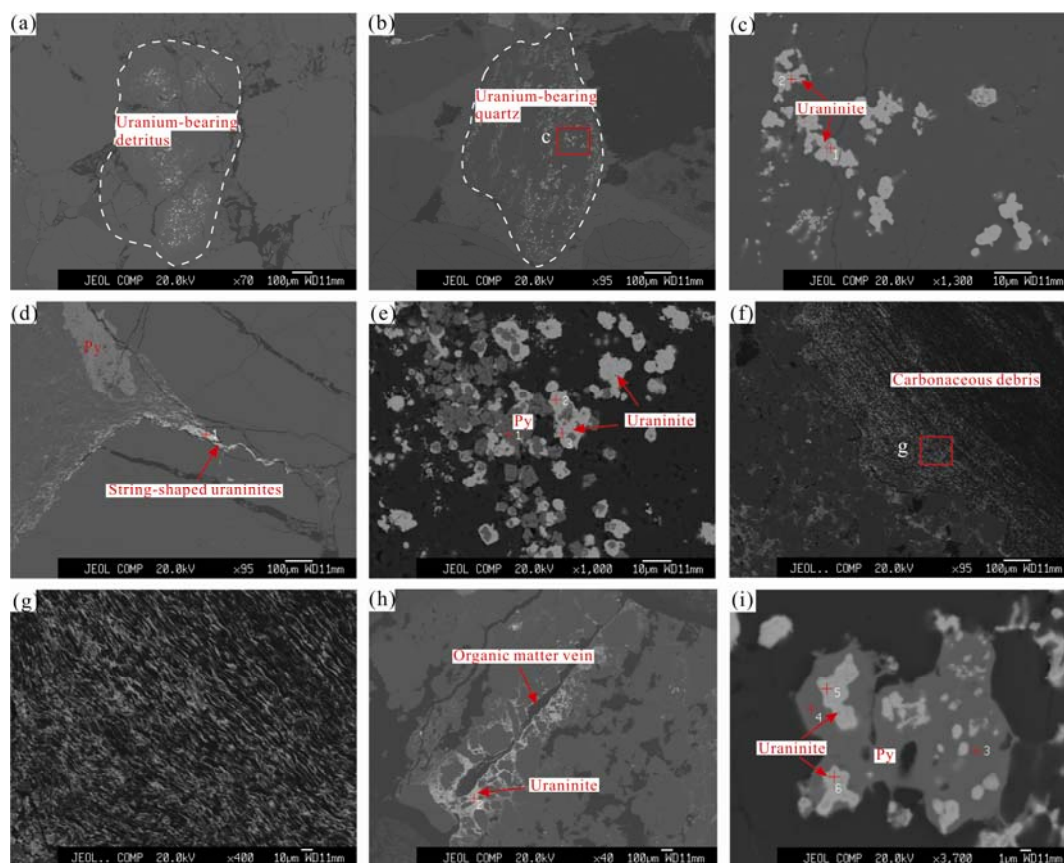


Fig. 7. Uranium mineralization types and spatial distribution of uraninite in the ores.

(a), Uranium-bearing detritus with brightly dotted uraninite. (b), Uranium-bearing metamorphic quartz with brightly dotted uraninite. (c), Micro-fine uraninite particles in the quartz detritus and electron microprobe measurement points. (d), String-shaped uraninite filling the intergranular pores and electron microprobe measurement point. (e), Uraninite precipitating around pyrite and electron microprobe measurement points. (f), Carbonaceous debris with bright uraninite. (g), Uraninite filling plant cells. (h), Uraninite cementing detritus and electron microprobe measurement point. (i), Uraninite in subhedral pyrite and electron microprobe measurement points.

**Table 2** The formation sequence of uranium and alteration minerals in the Sawafuqi uranium deposit

Mineralization stages	Uranium minerals	Alteration minerals	Major associated elements
Synsedimentary uranium pre-enrichment	Uraninite microparticle and aggregate in the detritus.	Carbonate and clay cement. Strawberry-like pyrite.	Si, Ca, Ti
Interlayer oxidation zone uranium mineralization	String-shaped uraninite filling intergranular pores or plant cells. Uranium absorbed by carbonaceous debris and clay.	Kaolinite replacing feldspar. Illite and I/S mixed layer replacing primary carbonaceous debris, matrix and other detritus.	Fe, S, Si
Vein-type uranium mineralization	Uraninite in cubic pyrite. Uraninite associated with silica-rich and organic matter veins.	Organic matter veins. Cubic and subhedral pyrite. Kaolinite. Chlorite replacing I/S mixed layer, primary carbonate and matrix. Silica-rich veins cutting string-shaped uraninite, organic matter veins and clay cement.	Si, Ti, Fe

uraninite occurs as irregular aggregates that are interpreted to have been transported from elsewhere and deposited. It is therefore referred to as the synsedimentary mineralization stage, which contributes to the early uranium pre-enrichment of the deposit.

Macroscopic observations suggest that there are numerous yellowish red interlayer oxidation residues in the grayish white host sandstones. It is interpreted that the interlayer oxidation zone has been bleached and replaced by intense kaolinization. Uranium mineralization is

attributed to infiltration by the interlayer oxidization groundwater and is closely associated with pyrite and carbonized plant debris, and is typically characterized by continuous string-shaped uraninite particles filling intergranular pores and forming the main uranium orebodies in the Sawafuqi uranium deposit.

Both macroscopic and microscopic observations suggest that the host rocks have suffered from silica-rich vein superimposition, with numerous silica-rich veins cutting organic matter veins or string-shaped uraninite

grains, and chloritization. The yellowish red interlayer oxidation zone was bleached by the silica-rich fluids. The uranium mineralization owing to such superimposition is mostly associated with the silica-rich veins and is characterized by high U and Ti, and low Fe content. The first two stages of uranium mineralization were superimposed by silica-rich veins that formed high-grade tabular uranium orebodies.

The three stages of uranium mineralization, especially the silica-rich vein superimposed uranium mineralization, are uncommon in sandstone-hosted uranium deposits. The Sawafuqi uranium deposit, in the Kurgan Intramontane Basin, is attributed to tectonic deformation and presumably is directly associated with the South Tian Shan orogeny.

## 6.2 Mesozoic–Cenozoic uplift and erosion in South Tian Shan

Gao Zhiyong et al. (2015) reviewed data and identified four uplift stages in the South Tian Shan Mountain since Mesozoic: (i) the first uplift occurred in Late Triassic–Early Jurassic approximately 220–180 Ma ago; (ii) the second uplift occurred in the Late Jurassic–Early Cretaceous approximately 150–100 Ma ago; (iii) the third uplift occurred in the Late Cretaceous–Eocene approximately 95–45 Ma ago; and (iv) the fourth uplift occurred in the Miocene–Quaternary approximately 25 Ma ago. The uranium mineralization ages for the different sandstone-hosted uranium deposits in intramontane basins and those adjacent to the Tian Shan Mountain from China to Central Asia are 76 Ma, 48–21.4 Ma, and 7 Ma (Chen Zuyi et al., 2010). These ages are interpreted to represent the tectonically quiescent stages, namely, the deplanation period after the uplift (Liu Hongxun et al., 2009; Chen Zuyi et al., 2010). Tectonically quiescent setting is favorable for long-term infiltration of uranium-bearing groundwater into host rocks and producing sandstone-hosted uranium deposits. It is thus proposed that the uranium mineralization was driven by the uplift.

## 6.3 Synsedimentary uranium pre-enrichment

The detritus of the host rocks of the Sawafuqi deposit comprises metamorphic rocks, volcanic rocks, and granites, pointing to complex sources. The Lower Sinian Sawafuqi Group outcrops in the provenance area and is observed in the Mansuertage Uplift to the south of the Sawafuqi uranium deposit. The group consists of thick-bedded siliceous rocks, siliceous–argillaceous slates, sandstones, metavolcanics, and meta-volcaniclastic rocks. These rocks have experienced fragmentation, sericitization, chloritization, epidotization, and silicification to varying degrees. Two uranium occurrences

and numerous uranium anomalies developed in the silicified fracture zones. Furthermore, previous investigations have confirmed the high uranium content of the Lower Sinian Sawafuqi Group (21.1–194.9 ppm, with an average uranium content of 61.2 ppm) (Liu Zhangyue, 2008a). It is assumed that the uranium enrichment and mineralization occurred in this stratum during the orogeny related to the accretion of the Qiangtang Block to the southern Tarim Plate and rejuvenation of the Tian Shan orogenic belt (Yin et al., 1988; Graham et al., 1993), which was induced by tectonic-thermal events occurred in South Tian Shan during Triassic period (Hendrix et al., 1994; Lu et al., 1994; Greene et al., 2005; Jolivet et al., 2010). The orogeny subsequently uplifted the Lower Sinian Sawafuqi Group and made it an important source for the Jurassic strata in the Kurgan Intramontane Basin. At the beginning of Jurassic, the Sawafuqi area entered a period of sedimentation after the collision, with a high depositional rate (Jia et al., 1997; Liu Zhangyue et al., 2008b). Such tectonosedimentary features prevented the long-distance transport of the uranium-bearing detritus and consequently the oxidation or dissolution of uraninite. The rapid transport and deposition of uranium-bearing detritus produced the synsedimentary uranium pre-enrichment of the Sawafuqi uranium deposit.

## 6.4 Interlayer oxidation zone uranium mineralization

Driven by the Kohistan–Dras event in Late Cretaceous, tectonic uplift occurred in the northern margin of the Tarim Basin during the Paleocene (Li et al., 2004; Liu Hongxu et al., 2009; Yu et al., 2014; Yang et al., 2017), when the F1 fault was reactivated and tilted the piedmont Middle–Lower Jurassic host rocks, producing a sloped belt favorable for uranium mineralization. The long-term deplanation during Eocene–Oligocene after the Tian Shan Mountain uplift in the Paleocene caused extensive deposition of shallow lacustrine clastic rocks in the northern margin of the Tarim Basin (Li and Peng, 2010; Yu et al., 2014). Therefore, the Eocene–Oligocene tectonic environment was relatively quiet and conducive to long-term interlayer infiltration and oxidization by uranium-bearing underground water in the host rocks, which provided a stable time interval for interlayer oxidation zone and uranium mineralization. U–Pb ages for the Sawafuqi uranium deposit are 38.9 Ma and 6.6 Ma (Liu Hongxu et al., 2009). The former was from the uranium ore without silica-rich veins, whereas the latter was from the uranium ore with silica-rich veins.

Fluids flowing through the provenance area were rich in  $\text{HCO}_3^{3-}$  and slightly alkaline and could dissolve and transport uranyl carbonate ions, such as  $\text{UO}_2(\text{CO}_3)_2^{2-}$  and  $\text{UO}_2(\text{CO}_3)_3^{4-}$ . The uranium-bearing oxygenated fluids

permeated the interlayer sandstones that were rich in pyrite and carbonaceous debris. Sulfuric and organic acids were produced respectively, which lowered the fluid pH from weakly alkaline to weakly acidic and leached the plagioclase and potassium feldspar grains, producing kaolinization and illitization in the ore. Moreover, as the free oxygen in the fluids was exhausted, the high-valence uranium ( $U^{6+}$ ) and associated elements in the solution were reduced, concentrated, and precipitated during the relatively enclosed acidification process (Rackley, 1972). It was known from the  $\alpha$ -track radiography that the carbonaceous debris and clay minerals in the ore absorbed small quantities of uranium that together with uraninite formed the main uranium mineralization stage.

### 6.5 Formation of the vein-type uranium mineralization

Since the Miocene, especially the Pliocene, the collision between the Indian and Eurasian Plates led the northern margin of Tarim Basin to enter a period of strong tectonic deformation (Hendrix et al., 1994; Yang et al., 2017), when the F1 piedmont thrust fault caused the severe deformation of the Middle–Lower Jurassic host rocks and produced stockwork fractures in the Sawafuqi uranium deposit. The fractures in the coal-bearing clastic rocks are mainly filled by organic matter, whereas those adjacent to the F1 fault in Carboniferous and Jurassic strata are filled by silica-rich veins. The above suggest that owing to the intense intracontinental orogeny, deep hydrothermal fluids migrated upward along the F1 fault and altered the coal seams, accelerating the thermal evolution of the coal measures and generating hydrocarbons. The organic matter veins in the coal-bearing clastic rocks may be the product of the thermal metamorphism of the coal seams. According to Grayer (1998), the temperature of the fluids draining from the collisional orogenic belt to the basin can be as high as 300°C, leading coal to progressively change from bituminous coal to anthracite. The vitrinite reflectance (Ro) in the mining area is 0.42%–0.90% (Lu Xiuxiang et al., 2006; Liu Zhangyue et al., 2011), presumably, owing to the non-uniform thermal alteration of the coal seams. Altered by the hydrothermal fluids, the coal seams generated coal-derived liquid hydrocarbons that penetrated into the sandstones adjacent to the coal seams, further dissolving the feldspar grains in the host rocks and forming kaolinite. The latter covered the earlier red or yellowish red interlayer oxidation zone, causing it to fade and bleach (Beitler et al., 2003; Parry et al., 2004). In addition, the hydrothermal fluids altered the interlayer oxidation zone, forming a stockwork of silica-rich veins, quartz overgrowths, organic matter veins, and chlorite alteration in the ore-bearing sandstones. It subsequently led to the uranium redistribution, and thus formed the

tabular, stratiform, and lens-like orebodies. The 6.6 Ma is inferred to be the age of the superimposed epithermal uranium mineralization.

## 7 Conclusions

Significantly different from typical interlayer oxidation zone sandstone-hosted uranium deposits, the Sawafuqi uranium deposit is located in the tectonically active area within South Tian Shan, where the uranium orebodies are tabular, stratiform, quasi-stratiform, and lens-like and are characterized by high-grade uranium ore (locally more than 1.0%). Uranium mineralization is closely associated with pyrite and organic matter, especially in scattered anhedral (or subhedral) pyrite and organic matter veins. The mineralization-related alteration in the uranium ores includes kaolinization, illitization, chloritization, and silicification.

The microscopic observations of the uranium ore, combined with EPMA and  $\alpha$ -track radiography, identified three stages of uranium mineralization in the Sawafuqi uranium deposit: (i) uranium-bearing detritus and synsedimentary pre-enrichment; (ii) interlayer oxidation zone uranium mineralization; and (iii) vein-type uranium mineralization. Uraninite in the uranium-bearing detritus is of high purity, with the  $UO_2$  content of 78.1%–92.9%, whereas uraninite formed by the interlayer oxidation zone is of low purity and has high Fe content. Uraninite associated with silica-rich veins is pure and Ti-rich. The primary synsedimentary mineralization stage is responsible for the early uranium pre-enrichment. The interlayer oxidation formed the major uranium orebodies, and the late epithermal fluids redistributed the uranium minerals and formed the superimposed enrichment.

Tectonic activity drove the three stages of uranium mineralization in the Sawafuqi uranium deposit. In the Triassic, the Sinian Sawafuqi Group, with uranium-rich strata, started to uplift and was the main source for the Middle–Lower Jurassic sediments. The rapid transport and deposition of the uranium-bearing detritus resulted in the synsedimentary uranium pre-enrichment of the Sawafuqi uranium deposit. During the Eocene–Oligocene, the stable tectonic setting favored the long-term infiltration of uranium-bearing underground water that produced the interlayer oxidation zone and the associated uranium mineralization. Since the Miocene, the South Tian Shan entered a period of intense orogeny, and hydrothermal fluids migrated into the host rocks and redistributed the previously formed uranium orebodies, forming numerous silica-rich veins and superimposed uranium mineralization.

## Acknowledgments

This study was supported by the National Key Basic Research Program of China (No. 2015CB453004) and National Pre-research Project (No. 3210402). The authors are grateful to two reviewers for their constructive comments. In addition, special thanks are given to the associate editor: Prof. Chi Guoxiang who helpfully improves the quality of the paper.

Manuscript received Aug. 7, 2016

accepted Aug. 10, 2017

edited by Liu Lian

## References

- Alekandre, P., Kyser, K., Polito, P., and Thomas, D., 2005. Alteration mineralogy and stable isotope geochemistry of paleoproterozoic basement hosted unconformity-type uranium deposits in the athabasca basin, Canada. *Economic Geology*, 100(8): 1547–1563.
- Beitler, B., Chan, M.A., and Parry, W.T., 2003. Bleaching of Jurassic Navajo sandstone on Colorado Plateau Laramide highs: Evidence of exhumed hydrocarbon supergiants?. *Geology*, 31(12): 1041–1044.
- Biske, J.S., and Seltmann, R., 2010. Paleozoic Tian Shan as a transitional region between the Rheic and Urals-Turkestan oceans. *Gondwana Research*, 17: 602–613.
- Bonnetti, C., Liu Xiaodong, Yan Zhaobin, Cuney, M., Michels, R., Malartre, F., and Cai Jiangfang, 2017. Coupled uranium mineralisation and bacterial sulphate reduction for the genesis of the Baxingtu sandstone-hosted U deposit, SW Songliao Basin, NE China. *Ore Geology Reviews*, 82: 108–129.
- Bullen, M.E., Burbank, D.W., Garver, J.I., and Abdrakhmatov, K.Y., 2001. Late Cenozoic tectonic evolution of the northwestern Tien Shan: New age estimates for the initiation of mountain building. *Geological Society of America Bulletin*, 113(12): 1544–1559.
- Cao, B.F., Bai, G.P., and Zhang, K.X., 2016. A comprehensive review of hydrocarbons and genetic model of the sandstone-hosted Dongsheng uranium deposit, Ordos Basin, China. *Geofluids*, 16(3): 624–650.
- Charvet, J., Shu Liangshu, Laurent-Charvet, S., Wang Bo, Michel, F., Dominique, C., Chen Yan and Koen, D.J., 2011. Palaeozoic tectonic evolution of the Tianshan belt, NW China. *Science China Earth Sciences*, 54(2): 166–184.
- Chen Hongbin, Xu Gaozhong, Yang Mingli, Wang Jinping, Li Weihong and Quan Jianping, 2007. Direct Evidences for Reduction of Pitchblende by Pitch in the Sawapuqi Uranium Deposit, Xinjiang. *Bulletin of Mineralogy, Petrology and Geochemistry*, 26(3): 245–248 (in Chinese with English abstract).
- Chen Zuyi, Chen Daisheng, Gu Kangheng and Wang Yajing, 2010. The regional distribution regularities of ore-hosting horizon, deposit type and mineralization age of China's sandstone-hosted uranium deposits. *Uranium Geology*, 26(6): 321–330 (in Chinese with English abstract).
- Chi Guoxiang and Xue Chunji, 2014. Hydrodynamic regime as major control on localization of uranium mineralization in sedimentary basins. *Science China Earth Sciences*, 57: 2928–2933.
- Crawley, R.A., Holen, H.K., and Chenoweth, W.L., 1985. *Geology and application of geologic concepts, Morrison Formation. Grants Uranium Region, New Mexico, USA. Geological environments of sandstone-type uranium deposits.* Vienna: IAEA, TECDOC-328: 99–214.
- Deng Jun, Yang Liqiang, Zhai Yusheng, Sun Zhongshi and Chen Xueming, 2000. Theoretical framework and methodological system of tectonics-fluids-mineralization system and dynamics. *Earth Science-Journal of China University of Geosciences*, 25(1): 71–78 (in Chinese with English abstract).
- Devoto, R.H., 1978. Uranium in Phanerozoic sandstone and volcanic rocks. Short course in uranium deposits: *Their mineralogy and origin: Mineralogical Association of Canada, Short Course Handbook*, 3: 293–305.
- Du Letian and Ou Guangxi, 2007. Genetic relationship between basin formation, associated mineralization and mantle fluids. *Earth Science Frontiers*, 14(2): 215–224 (in Chinese with English abstract).
- Fang Minqiang, 2010. Analysis of metallogenetic characteristics and ore-controlling features of Sawafuqi uranium deposit. *West-China Exploration Engineering*, 22(7): 141–143 (in Chinese with English abstract).
- Fuchs, S., Schumann, D., Williams-Jones, A.E., and Vali, H., 2015. The growth and concentration of uranium and titanium minerals in hydrocarbons of the Carbon Leader Reef, Witwatersrand Supergroup, South Africa. *Chemical Geology*, 393–394: 55–66.
- Gao Jun, Klemd, R., Qian Qing, Zhang Xi, Li Jilei., Jiang Tuo and Yang Yaoqing, 2011. The collision between the Yili and Tarim blocks of the Southwestern Altaids: geochemical and age constraints of a leucogranite dike crosscutting the HP–LT metamorphic belt in the Chinese Tianshan Orogen. *Tectonophysics*, 499: 118–131.
- Gao Jun, Li Maosong, Xiao Xuchang, Tang Yaoqing and He Guoqi, 1998. Paleozoic tectonic evolution of the Tianshan orogen, northwestern China. *Tectonophysics*, 287: 213–231.
- Gao Zhiyong, Zhu Rukai, Feng Jiarui, Li Xiaopei, Zhao Xuesong and Guo Meili, 2015. Jurassic-Neogene conglomerate characteristics in Kuqa Depression and their response to tectonic uplifting of Tianshan Mountains. *Oil and Gas Geology*, 36(4): 534–544 (in Chinese with English abstract).
- Grayer, R., Garven, G., and Rickard, D., 1998. Fluid migration and coal-rank development in foreland basins. *Geology*, 26(8): 679–682.
- Graham, S.A., Hendrix, M.S., Wang, L.B., and Carroll, A.R., 1993. Collisional successor basins of western China: Impact of tectonic inheritance on sand composition. *Geological Society of America Bulletin*, 105(3): 323–344.
- Granger, H.C., Santos, E.S., Dean, B.G., and Moore, F.B., 1961. Sandstone-type uranium deposits at Ambrosia Lake, New Mexico; an interim report. *Economic Geology*, 56(7): 1179–1210.
- Granger, H.C., and Santos, E.S., 1986. Geology and ore deposits of the Section 23 mine, Ambrosia Lake district, New Mexico. In: Turner-Peterson, C.E. Santos, E.S. and Fishman, N.S. (eds.), *A basin analysis case study-the Morrison Formation, Grants Uranium Region, New Mexico*, AAPG, Studies in Geology no. 22: 185–210.
- Greene, T.J., Carroll, A.R., Wartes, M., Graham, S.A., and Wooden, J.L., 2005. Integrated provenance analysis of a

- complex orogenic terrane: Mesozoic uplift of the Bogda Shan and inception of the Turpan-Hami Basin, NW China. *Journal of Sedimentary Research*, 75(2): 251–267.
- Han Baofu, Guo Zhaojie, Zhang Zhicheng, Zheng Lei, Chen Jiafu and Song Biao, 2010. Age, geochemistry, and tectonic implications of a late Paleozoic stitching pluton in the North Tian Shan suture zone, western China. *Geological Society of America Bulletin*, 122: 627–640.
- Harshman, E.N., 1972. Geology and uranium deposits, Shirley Basin area, Wyoming. US. *Geological Survey Professional Paper*, 745, 82.
- He Guoqi, Li Maosong and Han Baofu, 2001. Geotectonic research of southwest Tianshan and its west adjacent area, China. *Xinjiang Geology*, 19(1): 7–11 (in Chinese with English abstract).
- Hendrix, M.S., Dumitru, T.A., and Graham, S.A., 1994. Late Oligocene-early Miocene unroofing in the Chinese Tian Shan: An early effect of the India-Asia collision. *Geology*, 22(6): 487–490.
- Hendrix, M.S., 2000. Evolution of Mesozoic sandstone compositions, southern Junggar, northern Tarim, and western Turpan basins, Northwest China: a detrital record of the ancestral Tian Shan. *Journal of Sedimentary Research*, 70(3): 520–532.
- Hou Zengqian, Yang Zhusen, Li Yinqing, Zeng Pusheng, Meng Yifeng, Xu Wenyi and Tian Shihong, 2004. Large-scale migration of fluids towards foreland basins during collisional orogeny: evidence from Triassic anhydrock sequences and regional alteration in Middle-Lower Yangtze area. *Mineral Deposits*, 23(3): 310–326 (in Chinese with English abstract).
- Hou Zengqian, 2010. Metallogensis of continental collision. *Acta Geologica Sinica*, 84(1): 30–58 (in Chinese with English abstract).
- Jaireth, S., McKay, A., and Lambert, I., 2008. Association of large sandstone uranium deposits with hydrocarbons. *AUSGEO News*, 89: 1–6.
- Jia Chengzao, 1997. *Structural characteristics and petroliferous features of Tarim Basin*. Beijing: Petroleum industry press, 348–364.
- Jiao Yangquan, Wu Liqun, Rong Hui, Peng Yunbiao, Miao Aisheng and Wang Xiaoming, 2016. The Relationship between Jurassic Coal Measures and Sandstone-type Uranium Deposits in the Northeastern Ordos Basin, China. *Acta Geologica Sinica* (English Edition), 90(6): 2117–2132.
- Jin Ruoshi, Zhang Chengjiang, Feng Xiaoxi, Tangchao, Zhu Qiang and Li Guangyao, 2014. The influence of fluid mixing on the mineralization of sandstone type uranium deposits. *Geological Bulletin of China*, 33(2): 354–358 (in Chinese with English abstract).
- Jolivet, M., Dominguez, S., Charreau, J., Chen Yan, Li Yongan and Wang Qingchen, 2010. Mesozoic and Cenozoic tectonic history of the Central Chinese Tian shan: Reactivated tectonic structures and active deformation. *Tectonics*, 29(6): 1–70.
- Komninou, A., and Sverjensky, D.A., 1995. Hydrothermal alteration and the chemistry of ore-forming fluids in an unconformity-type uranium deposit. *Geochimica Et Cosmochimica Acta*, 59(13): 2709–2723.
- Leach, D.L., Sangster, D.F., Kelley, K.D., Large Ross, R., Garven, G., and Allen, C.R., 2005. Sediment-hosted Pb-Zn Deposits: a global perspective. *Economic Geology*, 100: 561–608.
- Li Zhong and Peng Shoutao, 2010. Detrital zircon geochronology and its provenance implications: responses to Jurassic through Neogene basin-range interactions along northern margin of the Tarim Basin, Northwest China. *Basin Research*, 22: 126–138.
- Li Zhong, Song Wenjie, Peng Shoutao, Wang Daoxuan and Zhang Zhongpei, 2004. Mesozoic-Cenozoic tectonic relationships between the Kuqa Subbasin and Tian Shan, northwest China: constraints from depositional records. *Sedimentary Geology*, 172: 223–249.
- Li Ziyang, Fang Xiheng, Xia Yuliang, Xiao Xinjian, Sun Ye, Chen Anping, Jiao Yangquan, Zhang Ke and Abdrakhmatov, K.Y., 2005. Metallogenic conditions and exploration criteria of Dongsheng sandstone type uranium deposit in Inner Mongolia, China. In: Mao, J.W. and Bierlein, F.P. (eds.), *Mineral Deposit Research*, Springer: 291–294.
- Li Ziyang, Chen Anping, Fang Xiheng, Ou Guangxi, Zhang Ke, Jiao Yangquan, Xia Yuliang, Chen Fazheng, Zhou Wenbin, Liu Zhonghou, Wu Rengui, Xiao Xinjian and Sun Ye, 2006. Metallogenic mechanism and superposition metallogenic model of the sandstone type uranium deposits in northeastern Ordos Basin. *Mineral Deposits*, 25(S1): 245–248 (in Chinese with English abstract).
- Li Ziyang, Fang Xiheng, Chen Anping, Ou Guangxi, Xiao Xinjian, Sun Ye, Liu Chiyang and Wang Yi, 2007. Origin of gray-green sandstone in ore bed of sandstone type uranium deposit in north Ordos Basin. *Science in China Series D: Earth Sciences*, 50(S2): 165–173.
- Lin Xiaobin, Hao Weilin and Wang Zhiming, 2013. Analysis on paleo-hydrogeological conditions of uranium formation in Sawafuqi uranium deposit. *World Nuclear Geoscience*, 30(2): 98–102 (in Chinese with English abstract).
- Liu Hongxu, Dong Wenming, Liu Zhangyue and Chen Xiaolin, 2009. Mesozoic-Cenozoic tectonic evolution and its relation to sandstone-type uranium mineralization in northern Tarim area-Evidence from apatite fission track. *World Nuclear Geoscience*, 26(3): 125–133 (in Chinese with English abstract).
- Liu Zhangyue, 2008a. *The relationship between tectonic evolution and uranium ore formation of sandstone type in Sawabuqi area, Xinjiang*. Beijing: CNNC Beijing Research Institute of Uranium Geology (M.S thesis): 1–83 (in Chinese with English abstract).
- Liu Zhangyue, Dong Wenming, Qin Mingkuan and Chen Xiaolin, 2008b. Relationship between Jurassic sedimentary characteristics and uranium metallogenesis in Sawabuqi area, Xinjiang. *World Nuclear Geoscience*, 25(2): 73–78, 85 (in Chinese with English abstract).
- Liu Zhangyue, Dong Wenming and Liu Hongxu, 2011. Analysis on genesis of uranium-bearing coal in Sawabuqi area, Xinjiang. *Uranium Geology*, 27(6): 345–351 (in Chinese with English abstract).
- Lu Huafu, Howell, D.G., and Jia Dong, 1994. Rejuvenation of the Kuqa foreland basin, northern flank of the Tarim basin, Northwest China. *International Geology Review*, 36: 1151–1158.
- Lu Xiuxiang, Zhou Jinyuan, Yang Minghui, Ma Yujie and Zhang Cun, 2006. Oil and gas exploration prospect in Wushi sag and Wensu uplift of Tarim Basin. *Journal of China University of Petroleum*, 30(1): 17–21 (in Chinese with English abstract).
- Nutt, C.J., 1989. Chloritization and associated alteration at the

- jabiluka unconformity-type uranium deposit, northern territory, australia. *Canadian Mineralogist*, 27(S4): 41–58.
- Nie Fengjun, Lin Shuangxing, Yan Zhaobin, Rao Minghui, Yang Yongji, Zhang Chengyong and Yan Yongjie, 2010. Hydrothermal Mineralization of Uranium in Sandstone, Teguida, Niger. *Acta Geoscientia Sinica*, 31(6): 819–831 (in Chinese with English abstract).
- Mitchell, A.H.G., and Garson, M.S., 1981. *Mineral deposits and global tectonic settings*. London: Academic Press, 1–266.
- OECD/NEA-IAEA. 2008. Uranium 2007: Resources, Production and Demand, 2007 RedBook. Nuclear Energy Agency, 391.
- Oliver, J., 1992. The spots and stains of plate tectonics. *Earth-Science Reviews*, 32(1–2): 77–106.
- Parry, W.T., Chan, M.A., and Beitler, B., 2004. Chemical bleaching indicates episodes of fluid flow in deformation bands in sandstone. *AAPG Bulletin*, 88(2): 175–191.
- Polito, P.A., Kyser, T.K., and Jackson, M.J., 2006. The role of sandstone diagenesis and aquifer evolution in the formation of uranium and zinc-lead deposits, southern mearthur basin, northern territory, australia. *Economic Geology*, 101(6): 1189–1209.
- Rackley, R.I., 1972. Environment of Wyoming Tertiary uranium deposits. *AAPG Bulletin*, 56(4): 755–774.
- Rieger, A., Schwark, L., Cisternas, M.I.A., and Miller, H., 2008. Genesis and evolution of Bitumen in Lower Cretaceous lavas and implications for strata-bound copper deposits, North Chile. *Economic Geology*, 103(2): 387–404.
- Saucier, A.E., 1980. Tertiary oxidation in Westwater Canyon member of Morrison formation. In: Rautman, C.A. (ed.), *Geology and mineral technology of the Grants Uranium Region 1979*. New Mexico Bureau of Geology & Mines Mineral Resources, Memoirs 38: 151–157.
- Shawe, D.R., 1956. Significance of roll ore bodies in genesis of uranium-vanadium deposits on the Colorado Plateau. In: Page, L.R. Stocking, H.E. Smith, H.B. and D., J.F. (eds.), *Contributions to the geology of uranium and thorium*. US Geological Survey Professional Paper, 300: 239–241.
- Shen Pingxi, 2010a. Metallogenic conditions and prospecting potential in Sawafuqi uranium deposit. *World Nuclear Geoscience*, 27(3): 139–143 (in Chinese with English abstract).
- Shen Pingxi, 2010b. Study on ore-bearing sandstone feature of Sawafuqi uranium deposit, Wensu county, Xinjiang. *West-China Exploration Engineering*, 22(8): 169–172 (in Chinese with English abstract).
- Shu Liangshu, Charvet, J., Lu Huafu and Laurent-Charvet, S., 2002. Paleozoic accretion-collision events and kinematics of ductile deformation in the central-southern Tianshan Belt, China. *Acta Geologica Sinica* (English Edition), 76(3): 308–323.
- Smieja-Król, B., Duber, S., and Rouzaud, J., 2009. Multiscale organisation of organic matter associated with gold and uranium minerals in the Witwatersrand basin, South Africa. *International Journal of Coal Geology*, 78: 77–88.
- Turner-Peterson, C.E., and Fishman, N.S., 1986. Geologic synthesis and genetic models for uranium mineralization in the Morrison Formation, Grants Uranium Region, New Mexico. In: Turner-Peterson, C.E. Santos, E.S. and Fishman, N.S. (eds.), *A basin analysis case study: the Morrison Formation, Grants Uranium Region, New Mexico*, AAPG Studies in Geology, 22: 357–388.
- Wright, R.J., 1955. Ore controls in sandstone uranium deposits of the Colorado Plateau. *Economic Geology*, 50(2): 135–155.
- Wu Bolin, Liu Chiyang and Wang Jianqiang, 2007. Basic characteristics of fluid geologic process of interlayer oxidation zone sandstone-type uranium deposit. *Science in China* (Series D), 50: 185–194.
- Wu Kongyun, Gao Lipeng and Shen Pingxi, 2010. Geochemical features of the interlayer oxidation zone in Sawafuqi uranium deposit. *World Nuclear Geoscience*, 27(3): 134–138, 148 (in Chinese with English abstract).
- Yang Wei, Li Jianfeng, Guo Zhaojie, Jolivet, M., and Heilbronn, G., 2017. New apatite fission-track ages of the western kuqa depression: implications for the mesozoic–cenozoic tectonic evolution of south tianshan, xinjiang. *Acta Geologica Sinica* (English Edition), 91(2): 396–413.
- Yin, A., Nie, S., Craig, P., Harrison, T.M., Ryerson, F.J., Qin Xianglin and Yang Geng, 1998. Late Cenozoic tectonic evolution of the southern Chinese Tian Shan. *Tectonics*, 17(1): 1–27.
- Yu Shun, Chen Wen, Evans, N.J., McInnes, B.I.A., Yin Jiyuan, Sun Jingbo, Li Jie and Zhang Bin, 2014. Cenozoic uplift, exhumation and deformation in the north Kuqa Depression, China as constrained by (U–Th)/He thermochronometry. *Tectonophysics*, 630: 166–182.
- Zhai Yusheng, 1996. Problems in the study of structure-fluid-ore-forming processes. *Earth Science Frontiers*, 3(3–4): 230–236 (in Chinese with English abstract).
- Zhang Chengyong, Nie Fengjun, Hou Shuren, Deng Wei, Wang Junlin and Zhang Liang, 2015. Study on hydrothermal alteration and relation with uranium mineralization of the Tamusu exogenetic uranium deposit, Inner Mongolia, China. *Acta Mineralogica Sinica*, 35(1): 79–86 (in Chinese with English abstract).
- Zhang Long, Liu Chiyang, Fayek, M., Wu Bolin, Lei Kaiyu, Cun Xiaoli and Sun Li, 2017. Hydrothermal mineralization in the sandstone-hosted Hangjinqi uranium deposit, north Ordos Basin, China. *Ore Geology Reviews*, 80, 103–115.
- Zhu Wenbin, Wan Jinglin, Shu Liangshu, Zhang Zhiyong, Su Jinbao, Sun Yan, Guo Jichun and Zhang, Xueyun, 2008. Late Mesozoic thermotectonic evolution of the Jueltage Range, Eastern Xinjiang, Northwest China: Evidence from apatite fission track data. *Acta Geologica Sinica* (English Edition), 82 (2): 348–357.

#### About the first author

LIU Zhangyue, Male; born in 1981 in Chaohu City, Anhui Province; Ph.D candidate in service at China University of Mining and Technology (Beijing); senior engineer of Beijing Research Institute of Uranium Geology, CNNC. His current research mainly focuses on the metallogenesis of sandstone-hosted uranium deposits in the coal-bearing clastic rocks. E-mail: zhyueliu@163.com.